Pharmaceutical Research, Vol. 24, No. 6, June 2007 (© 2007)
DOI: 10.1007/s11095-007-9252-1

Research Paper

Noninvasive Visualization of Pharmacokinetics, Biodistribution and Tumor Targeting of Poly[*N*-(2-hydroxypropyl)methacrylamide] in Mice Using Contrast Enhanced MRI

Yanli Wang,[1] Furong Ye,[1] Eun-Kee Jeong,[2] Yongen Sun,[1] Dennis L. Parker,[2] and Zheng-Rong Lu[1,3]

Received December 1, 2006; accepted January 26, 2007; published online March 27, 2007

Purpose. To study a non-invasive method of using contrast enhanced magnetic resonance imaging (MRI) to visualize the real-time pharmacokinetics, biodistribution and tumor accumulation of paramagnetically labeled poly[*N*-(2-hydroxypropyl)methacrylamide] (PHPMA) copolymer conjugates with different molecular weights and spacers in tumor-bearing mice.
Materials and Methods. Paramagnetically labeled HPMA copolymer conjugates were synthesized by free radical copolymerization of HPMA with monomers containing a chelating ligand, followed by complexation with $Gd(OAc)_3$. A stable paramagnetic chelate, Gd-DO3A, was conjugated to the copolymers via a degradable spacer GlyPheLeuGly and a non-degradable spacer GlyGly, respectively. The conjugates with molecular weights of 28, 60 and 121 kDa and narrow molecular weight distributions were prepared by fractionation with size exclusion chromatography. The conjugates were injected into athymic nude mice bearing MDA-MB-231 human breast carcinoma xenografts via a tail vein. MR images were acquired before and at various time points after the injection with a 3D FLASH sequence and a 2D spin-echo sequence at 3T. Pharmacokinetics, biodistribution and tumor accumulation of the conjugates were visualized based on the contrast enhancement in the blood, major organs and tumor tissue at various time points. The size effect of the conjugates was analyzed among the conjugates.
Results. Contrast enhanced MRI resulted in a real-time, three-dimensional visualization of blood circulation, pharmacokinetics, biodistribution and tumor accumulation of the conjugates, and the size effect on these pharmaceutical properties. HPMA copolymer conjugates with high molecular weight had a prolonged blood circulation time and high passive tumor targeting efficiency. Non-biodegradable HPMA copolymers with molecular weights higher than the threshold of renal filtration demonstrated higher efficiency for tumor drug delivery than biodegradable poly(*L*-glutamic acid).
Conclusions. Contrast enhanced MRI is an effective method for non-invasive visualization of *in vivo* properties of the paramagnetically labeled polymer conjugates in preclinical studies.

KEY WORDS: conjugates; drug delivery; magnetic resonance imaging (MRI); non-invasive visualization; poly[*N*-(2-hydroxypropyl)methacrylamide] (PHPMA).

INTRODUCTION

N-(2-Hydroxypropyl)methacrylamide (HPMA) copolymer is a biocompatible, water-soluble, inert and neutral drug carrier for *in vivo* delivery of anti-cancer therapeutics (1,2). The conjugation of anticancer drugs to HPMA copolymers results in many advantageous features over small molecular therapeutics, including improved solubility and bioavailability, preferential accumulation of the conjugates in solid tumors or passive tumor targeting due to the enhanced permeability and retention (EPR) effect (3), reduced systemic toxicity and enhanced therapeutic efficacy, and down-regulation of multi-drug resistance (1). Several HPMA copolymer-anticancer drug conjugates are now in various stages of preclinical and clinical studies (4). Traditionally, the pharmacokinetics and drug delivery efficiency of polymer conjugates are investigated by surgery-based methods in the preclinical studies. These methods are invasive and a large number of experimental animals are sacrificed during these studies (5). Biomedical imaging techniques provide a valuable tool to non-invasively visualize the *in vivo* pharmaceutical and pharmacological properties of therapeutics and their delivery systems in both preclinical and clinical studies.

The *in vivo* properties of polymer drug conjugates can be non-invasively investigated using imaging after they are labeled with imaging probes. HPMA copolymers and drug conjugates have been labeled with various radioactive imaging probes to non-invasively study the effect of size and structure on biodistribution and tumor accumulation in

[1] Department of Pharmaceutics and Pharmaceutical Chemistry, University of Utah, 421 Wakara Way, Suite 318, Salt Lake City, Utah 84108, USA.
[2] Department of Radiology, University of Utah, Salt Lake City, Utah 84108, USA.
[3] To whom correspondence should be addressed. (e-mail: ZhengRong.Lu@utah.edu)

both preclinical and clinical studies with gamma scintigraphy and SPECT (6–10). Gamma scintigraphy is quantitative and highly sensitive, but is limited by its low spatial resolution. Recently, it has been reported that HPMA copolymer conjugates were also labeled with an MRI contrast agent to non-invasively evaluate accumulation of HPMA copolymers in the arthritic joints of rats with contrast enhanced MRI (11). In comparison, contrast enhanced MRI provides three-dimensional images with high spatial resolution.

Previously, we studied size effect of paramagnetically labeled ionizable and biodegradable poly(*L*-glutamic acid) on *in vivo* drug delivery with non-invasive contrast enhanced MRI (12). Pharmacokinetic properties and biodistribution of the conjugates were visualized with high spatial resolution. Although contrast enhanced MRI is not quantitative, the conclusions drawn from the semi-quantitative imaging study about the size effect on *in vivo* drug delivery with polymer conjugates were consistent to those based on conventional methods. Here, we further studied the pharmacokinetics and *in vivo* tumor delivery of paramagnetically labeled non-degradable HPMA copolymer conjugates and the effect of size and spacer on these properties with dynamic contrast enhanced MRI in a small number of mice bearing MDA-MB-231 human breast carcinoma xenografts. Higher tumor targeting efficiency was observed for the HPMA copolymer conjugates than the biodegradable poly(*L*-glutamic acid) conjugates when their molecular weights were larger than the renal filtration threshold.

MATERIALS AND METHODS

Materials

N-(2-Hydroxypropyl)methacrylamide (HPMA), MA-GFLG-ONp, and MA-GG-ONp were prepared according to a published method (13). 1,4,7,10-Tetraazacyclododecane-1,4,7-tri(acetic acid)-10-(acetic acid-1,6-hexanediamine monoamide) and 1,4,7,10-tetraazacyclododecane-1,4,7-tri (acetic acid)-10-(acetic acid-1,6-ethylenediamine monoamide) were similarly prepared according to a published method (14). 2,2′-Azobisisobutyronitrile (AIBN) was obtained from Aldrich (Milwaukee, WI, USA). Bromoacetic acid, mono-N-*t*-Boc-1,6-hexanediamine, N-hydroxysuccinimide (NHS) and N-diisopropylethylamine (DIPEA) were purchased from Lancaster Synthesis, Inc (Pelham, NH). 1,4,7,10-Tetraazacyclododecane (cyclen) was purchased from Macrocyclics (Dallas, TX). Gadolinium(III) acetate and *tert*-butyl bromoacetate were purchased from Alfa Aesar (Ward Hill, MA). Optima nitric acid was purchased from Fisher Chemical (Pittsburgh, PA). The MDA-MB-231 human breast cancer cell line, Leibovitz's L-15 medium with 2 mM *L*-glutamine, and FBS were purchased from the American Type Culture Collection (ATCC, Manassas, VA). Matrigel was purchased from BD Biosciences (San Jose, CA).

Synthesis of N-Methacryloylglycylglycyl-1,6-Hexanediamine-DO3A (MA-GG-DO3A)

MA-GG-ONp (0.28 g, 0.87 mmol), 1,4,7,10-tetraazacyclododecane-1,4,7-tri(acetic acid)-10-(acetic acid-1,6-hexanediamine monoamide) trifluoroacetic acid salt (equal molar) and an inhibitor *tert*-octyl pyrocatechin were dissolved in anhydrous DMF. N-Diisopropylethylamine (2.88 ml) was then added dropwise and the mixture was stirred at room temperature for 48 h. The solution was added dropwise to ether to precipitate the product. The precipitate was filtered, washed with ether, dried in vacuuo, resulting in MA-GG-DO3A in a yield of 85%. MA-GG-DO3A was used for copolymerization without further purification. ^{1}HNMR, δ_H (D_2O, ppm): 5.74 (s, 1H), 5.38 (s, 1H), 3.84 (s, 2H), 3.73 (s, 2H), 2.80–3.70 (28H, m), 1.80 (s, 3H) 1.25–1.30 (m, 4H), 1.10–1.20 (m, 4H). ESI-MS (m/z, M + H^+): 685.31 (measured), 685.38 (calculated).

Synthesis of N-Methacryloylglycylphenylalanylleucylglycyl-1,2-Ethylenediamine-DO3A (MA-GFLG-DO3A)

MA-GFLG-DO3A was prepared by the reaction of MA-GFLG-ONp and 1,4,7,10-tetraazacyclododecane-1,4,7-tri(acetic acid)-10-(acetic acid-1,2-ethylenediamine monoamide) trifluoroacetate according to the same procedure as MA-GG-DO3A. Yield: 86%. ^{1}HNMR, δ_H (CD_3OD, ppm): 7.20–7.32 (m, 5H), 5.78 (s, 1H), 5.43 (s, 1H), 4.58–4.68 (m, 1H), 4.30–4.38 (m, 1H), 2.90–3.95 (m, 34H), 1.98 (s, 3H), 1.60–1.72 (m, 3H), 0.89–0.98 m, 6H). ESI-MS (m/z, M + H^+): 945.5 (measured), 945.5 (calculated).

Preparation of Paramagnetically Labeled PHPMA Copolymer Conjugates

HPMA (0.169 g, 1.182 mmol), MA-GG-DO3A (0.270 g, 0.296 mmol), AIBN (7 mg) was dissolved in DMSO in an ampoule and purged with N_2 for 10 min. The ampoule was flame-sealed and maintained at 50°C for 24 h. The copolymer was isolated by precipitating the reaction solution into a mixture of acetone and ether (1:2). The copolymers were further purified by dialysis with Spectra/Por® 6 membrane (MWCO 6–8 kDa) against de-ionized water and lyophilized to give a colorless product (0.278 g). PHPMA-GG-DO3A and an excess of $Gd(OAc)_3$ were then dissolved in 2 ml water and stirred at 50°C for 48 h. The pH of the solution was maintained at 5.5–6.0 by addition of 0.01 N NaOH. EDTA dipotassium salt was then added into the solution to remove excess Gd^{3+} ions. The solution was then transferred into to a dialysis tube with Spectra/Por® 6 membrane (MWCO 6–8 kDa) and dialyzed against deionized water for 48 h. The residue was then filtered and lyophilized to give 0.239 g of final product PHPMA-GG-(Gd-DO3A) (54%). The gadolinium content was 0.51 mmol/g as determined by inductively coupled plasma optical emission spectroscopy (ICP-OES) (Perkin-Elmer, Norwalk, CT, Optima 3100XL). The weight average molecular weight of the polymer conjugates was 71.9 kDa with a polydispersity of 1.82 as determined by size exclusion chromatography (SEC) using the ÄKTA FPLC system (Amersham Pharmacia Biotech) equipped with UV and RI detectors, calibrated with PHPMA standards.

PHPMA-GFLG-(Gd-DO3A) was similarly prepared by free radical copolymerization of HPMA with MA-GFLG-DO3A, followed by complexation with $Gd(OAc)_3$. The weight average molecular weight of the copolymer conjugate

was 56.8 KDa with a polydispersity of 1.35. The Gd content in the conjugate was 0.393 mmol/g.

PHPMA-GG-(Gd-DO3A) and PHPMA-GFLG-(Gd-DO3A) conjugates were fractionated by SEC to prepare the conjugates with different molecular weights and narrow molecular weight distributions. The polymer conjugates were loaded to a ÄKTAprime plus system equipped with an XK50 preparative column (50 mm × 100 cm) packed with Superose 6 and eluted with PBS buffer (pH 7.4). The fractions were collected at various elution times and then dialyzed against de-ionized water and lyophilized. Average molecular weights and molecular weight distributions of the fractions were determined by analytical SEC. Gd content of the conjugate fractions was determined by ICP-OES at 342 nm. T_1 relaxivity of the conjugate fractions was measured by a standard inversion recovery sequence on a Siemens Trio 3T MRI scanner (15) and calculated from the T_1 relaxation times of three concentrations.

Animal Tumor Model

Human breast carcinoma cell line MDA-MB-231 was cultured in L-15 media supplemented with 2 μM glutamine and 10% FBS in 5% CO_2. Female athymic nu/nu mice (6 weeks old) were purchased from the National Cancer Institute (Frederick, MD). The mice were cared according to the guidelines of the IACUC, University of Utah. The mice were subcutaneously implanted in both lower flanks with 2×10^6 MDA-MB-231 cells in a mixture of 50 μl culture media and 50 μl Matrigel. MRI experiment was carried out when the tumor size reached 8–10 mm in diameter.

MR Imaging

The mice were anesthetized by intramuscular administration of a mixture of ketamine (45 mg/kg) and xylazine (6 mg/kg). The polymer conjugates were injected via a tail vein at a dose of 0.03 mmol-Gd/kg. Each molecular weight fraction was studied in a group of three mice. Contrast-enhanced images were acquired before and at various time points after injection on a Siemens Trio 3T MRI scanner using a human wrist coil. A 3D FLASH pulse sequence with 2.7 ms echo time (TE), 7.8 ms repetition time (TR), 25° RF tip angle, 120 mm field of view (FOV), and spatial resolution of $0.4 \times 0.4 \times 0.5$ mm^3 were used to acquire 3D MR images. A 2D spin echo sequence with 400 ms TR, 10 ms TE, 90° tip angle, 50 mm FOV, 2 mm slice thickness was also used to acquire 2D T_1 weighted axial tumor images after the acquisition of 3D MR images. MR images were acquired continuously for the first 20 min and then at 1, 2, 3, 4 and 24 h post-injection. For high molecular weight conjugates (60 and 121 kDa), MR images were also obtained at 48, 72 and 168 h post-injection. MR images were analyzed with Osirix (http://homepage.mac.com/rossetantoine/osirix/) software and IDL (Interactive Data Language, Boulder, CO). In each animal, the regions-of-interest (ROIs) were set at the kidneys, liver, lung, muscle, tumor tissues and blood in the heart. The liver ROIs were defined in the center of the tissue. For the blood in the heart, signal intensity (SI) in both chambers was similar and ROIs were defined in the left ventricular chamber. For tumor tissues, the ROIs of tumor periphery was defined along the tumor rim with a width of approximately 2 mm and tumor interstitium was defined in the tumor center core. Data analysis was performed by measuring average signal intensities in the ROIs before and after injection of contrast agents. The relative signal intensity was calculated for each mouse as relative $SI = SI_{post}/SI_{pre}$ and averaged over three mice. The 2D axial spin-echo MR images were processed by homemade software using IDL. Color-coding was implemented by applying a transparent image overlay. The transparent image was overlaid on top of the base image while transparency was set up using the ALPHA_CHANNEL property and a color table was applied.

Gd Biodistribution

The mice were sacrificed at the end of MRI studies, at 24 h post-injection for the conjugates of 28 kDa and on the seventh day after injecting the conjugates of 60 kDa and 121 kDa. Major organ and tissue samples, including the heart, liver, lung, spleen, kidneys, muscle and tumor tissue, were collected and weighted. The tissue samples were dissolved in 0.5 ml ultrapure nitric acid (70%), except the liver, which was dissolved in 1.0 ml nitric acid (70%). The resulting mixture was diluted 4–10 times with DI water depending on the organs or tissues and centrifuged at 14,000 rpm for 20 min. The supernatants were filtered through a 0.2 μm syringe filter, and Gd content was determined by ICP-OES (16). The Gd tissue retention was represented as percentage of injected dose (ID) per gram of organ or tissue.

Statistical analysis was performed using Prism software (Version 4.0b, GraphPad software Inc., San Diego, CA) using two-way repeated measures ANOVA. Bonferroni post-test was used to analyze the differences among the conjugates. Statistical differences were considered as significant when $p < 0.05$.

RESULTS

Paramagnetically labeled HPMA copolymer conjugates, poly[HPMA-co-(MA-GG-(Gd-DO3A))] (PHPMA-GG-(Gd-DO3A)) and poly[HPMA-co-(MA-GFLG-(Gd-DO3A))] (PHPMA-GFLG-(Gd-DO3A)), were synthesized by free radical copolymerization of HPMA and DO3A containing monomers, MA-GG-1,6-hexanediamine-DO3A and MA-GFLG-1,2-ethylenediamine-DO3A, respectively, followed by the complexation with $Gd(OAc)_3$. The structures of the labeled HPMA copolymer conjugates are shown in Fig. 1. A nondegradable spacer GG-1,6-hexanediamine and a degradable spacer GFLG-1,2-ethylenediamine were designed to study the effect of spacer degradability on *in vivo* release of Gd-DO3A from the conjugates. Different alkyldiamines were used to maintain a similar length of the spacers between the chelate and polymer chains. The copolymers had relatively broad molecular weight distributions after free radical polymerization and purification with dialysis. In order to accurately evaluate the size effect of the polymer conjugates on pharmacokinetics and *in vivo* tumor targeting efficiency, the copolymer conjugates were fractionated by size exclusion chromatography. The conjugate fractions with molecular weights of approximately 28, 60, and 121 kDa and

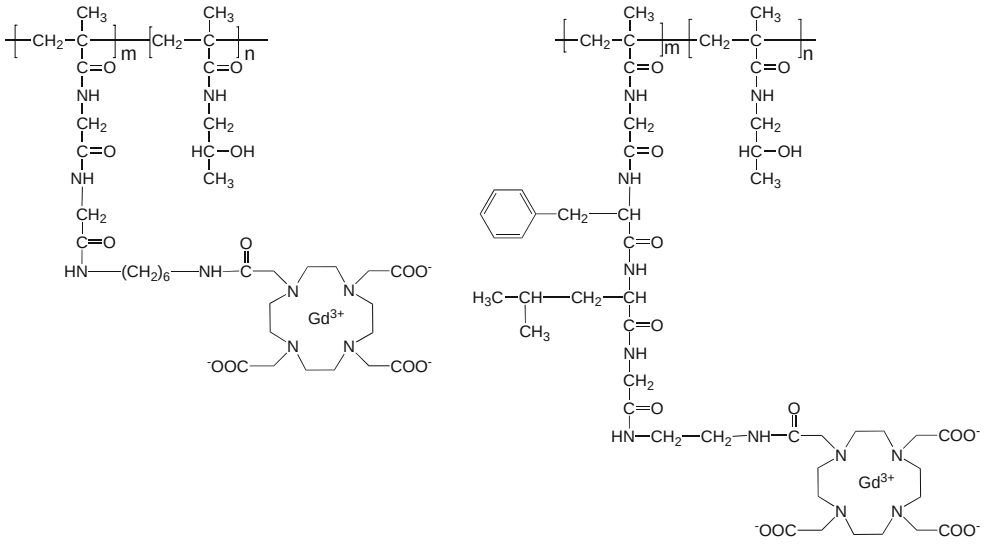

Fig. 1. Chemical structure of PHPMA-GG-1,6-hexanediamine-(Gd-DO3A) and PHPMA-GFLG-1,2-ethylenediamine-(Gd-DO3A).

narrow polydispersity ($M_w/M_n < 1.1$) were selected for non-invasive imaging study of size and structure effects of the conjugates on *in vivo* drug delivery. The fractions with molecular weight of approximately 28 kDa represented the conjugates with molecular weights below the threshold of renal glomerular filtration (ca. 45 kDa). Similarly, the fractions of 60 and 121 kDa represented the conjugates with medium and high molecular weights above the renal threshold. The physicochemical properties, including number and weight average molecular weights, Gd content and T_1 relaxivity (r_1), of the fractions are listed in Table I. It appears that the molecular weight and spacer of the conjugates did not significantly affect their relaxivity.

Figure 2 shows the representative three-dimensional maximum intensity projection (MIP) MR images of tumor bearing mice before and at various time points after the injection of the conjugates at a dose of 0.03 mmol-Gd/kg. Size-dependent blood pharmacokinetics of the conjugates was clearly shown in the dynamic MR images. Both low molecular weight conjugates (28 kDa) showed more rapid decrease of contrast enhancement in the blood than the 60 and 121 kDa conjugates. The signal intensity in the urinary bladder gradually increased over 4 h for the 28 kDa conjugates. The results indicate that the 28 kDa conjugates rapidly cleared from the blood circulation via renal filtration and accumulated in the urinary bladder. The contrast enhancement in the blood returned to precontrast level for the low molecular weight conjugates at 24 h post-injection. Therefore, no further MRI scans were performed for the 28 kDa conjugates. The prolonged blood circulation of the conjugates with higher molecular weights was clearly shown in the dynamic MR images. The high molecular weight conjugate (121 kDa) resulted in more prolonged strong contrast enhancement in the blood than the conjugates of the medium molecular weight (60 kDa). The conjugates of 121 kDa were still visible in the blood 72 h post-injection, when no enhancement was seen for the 60 kDa conjugates. Gradual increase of contrast enhancement was also observed in the urinary bladder of the mice injected with the 60 kDa conjugates, indicating that the linear polymer conjugates of the medium molecular weight can still be excreted via renal filtration, but at a slower rate. The blood signal intensity returned to the background level 7 days post-injection for all high molecular weight conjugates. The dynamic MR images clearly revealed that the HPMA copolymer conjugates with higher molecular weight had a longer blood circulation. It appears that the degradability of the spacers for Gd-DO3A did not have a significant impact on the blood pharmacokinetics of the conjugates as shown by contrast enhanced MRI.

The conjugates also showed size dependent dynamic accumulation in the liver. The dynamic changes of contrast enhancement of the conjugates in the liver were consistent to the size-dependent dynamic patterns in the blood. The enhancement in the liver was less significant than that in

Table I. Physicochemical Characteristics of PHPMA-Gd-DO3A Conjugate Fractions

	PHPMA-GG-Gd-DO3A			PHPMA-GFLG-Gd-DO3A		
	GG-28	GG-60	GG-121	GFLG-28	GFLG-60	GFLG-121
Gd-content (mmol/g)	0.44	0.47	0.43	0.36	0.37	0.39
r_1 (mM^{-1}/s^{-1})	11.7	10.9	10.7	11.9	10.9	11.5
M_w (kDa)	27.2	60.0	121	28.0	59.5	121
M_w/M_n	1.06	1.07	1.05	1.08	1.07	1.05

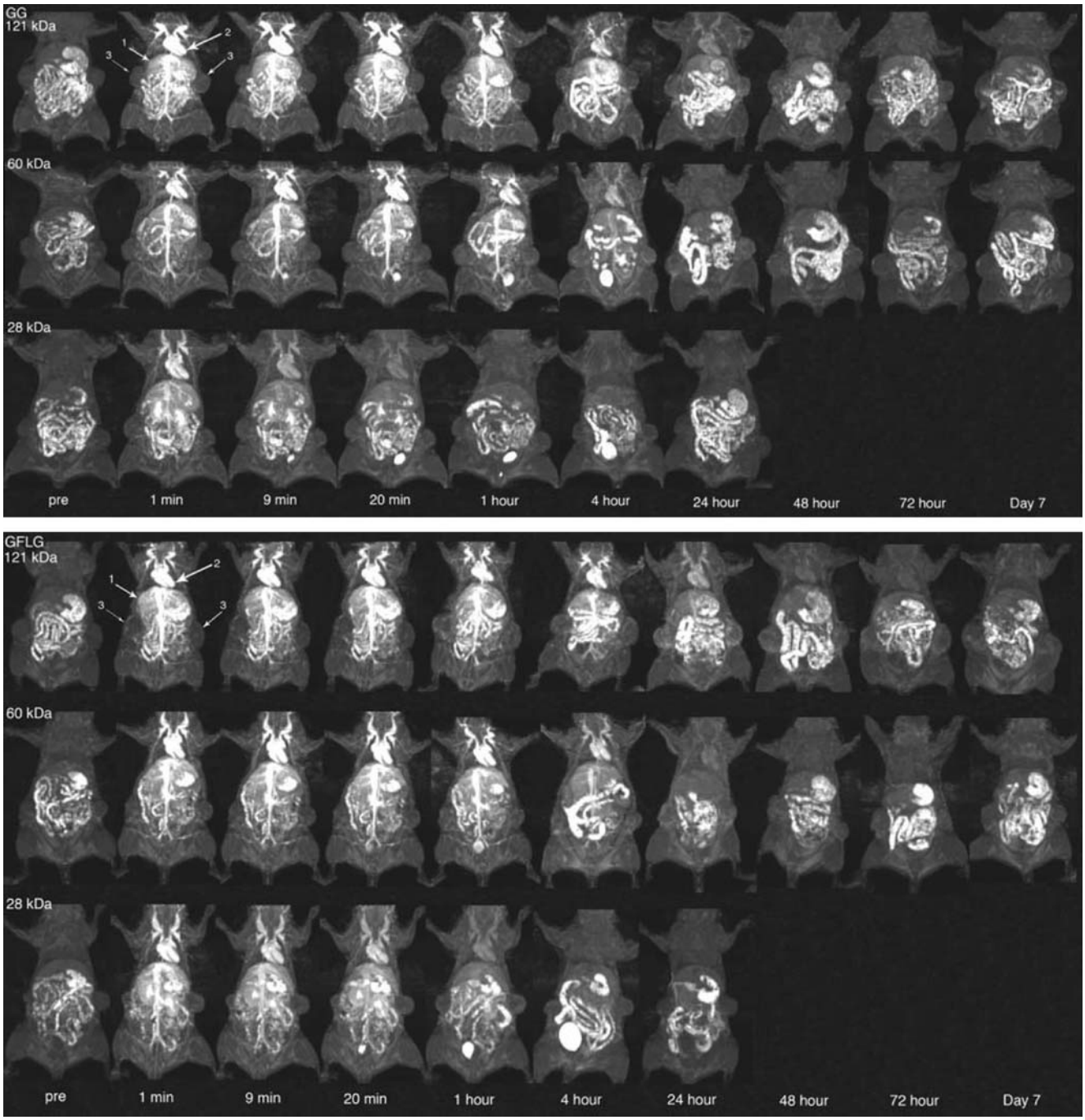

Fig. 2. Three-dimensional MIP MR images of mice bearing MDA-MB-231 human breast carcinoma xenografts injected with PHPMA-GG-1,6-hexanediamine-(Gd-DO3A) (GG) and PHPMA-GFLG-1,2-ethylenediamine-(Gd-DO3A) (GFLG) conjugates with molecular weights of 28, 60 and 121 kDa before contrast and at various time points after the injection of the conjugates at a dose of 0.03 mmol-Gd/kg. *Arrows* indicate the liver (1), heart (2), and tumor tissue (3).

the blood. It can be seen that the conjugates of 121 kDa had more prolonged liver retention than those of 60 and 28 kDa. The conjugates of 28 kDa had the least accumulation in the liver. Significant enhancement was still visible in the liver at least 3 days after the injection for the conjugates with the high molecular weight. The contrast enhancement in the lung was low as compared to other organs, possibly due to the presence of air.

Significant tumor enhancement was also observed in the 3D MR images for the conjugates, particularly for the conjugates with higher molecular weights. In order to clearly visualize the dynamic changes of tumor accumulation of different polymer conjugates, axial 2D T_1-weighted spin-echo images through tumor tissues were acquired before and at various time points after the injection of the conjugates. Figure 3 shows the color-coded axial spin-echo images of the tumor cross-sections highlighting the contrast enhancement, which can be correlated to the accumulation and distribution of the conjugates. Heterogeneous tumor accumulation of the conjugates was observed in all tumor tissues. The dynamic MR

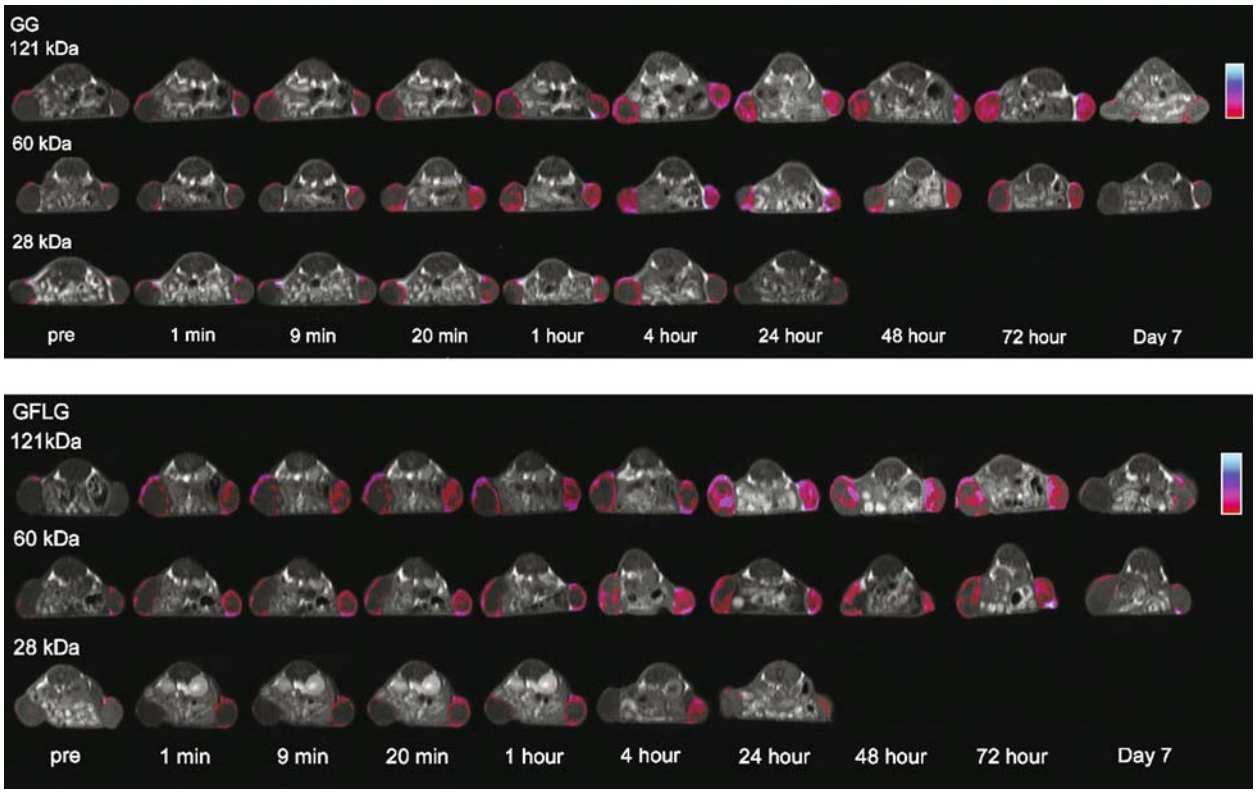

Fig. 3. Color-coded 2D axial spin-echo MR images of mice injected with PHPMA-GG-1,6-hexanediamine-(Gd-DO3A) (GG) and PHPMA-GFLG-1,2-ethylenediamine-(Gd-DO3A) (GFLG) conjugates with molecular weights of 28, 60 and 121 kDa before contrast and at various time points after the injection of the conjugates at a dose of 0.03 mmol-Gd/kg.

images revealed a gradual, size-dependent accumulation of conjugates in tumor tissues. Significant contrast enhancement was observed at tumor periphery during initial period after the injection for all conjugates. Polymer conjugates gradually accumulated in the tumor interstitium, resulting in significant contrast enhancement within the inner tumor tissue. It appears that polymer conjugates with higher molecular weights had higher passive tumor targeting efficiency. The conjugates of 121 kDa resulted in more significant and prolonged tumor enhancement than those of 60 and 28 kDa. Tumor enhancement with the 28 kDa Mw conjugates returned to the background level at 24 h postinjection, indicating poorer tumor targeting efficiency than that of the conjugates of 121 and 60 kDa.

Three-dimensional, whole body pharmacokinetics and biodistribution of the HPMA copolymer conjugates were clearly visualized by dynamic contrast enhanced MRI with high spatial resolution. Analysis of the signal intensities of the major organs, the blood and tumor provided semi-quantitative evaluation of the pharmacokinetics and biodistribution of the conjugates in these organs and tissues. The dynamic changes in the relative MR signal intensities, the ratio of post-contrast signal intensity to precontrast signal intensity, in the blood, liver, kidneys and tumor tissues were calculated and are plotted in Figs. 4 and 5. The relative signal intensities semi-quantitatively depicted the pharmacokinetics of the conjugates in the blood and major organs and the effect of polymer size on the pharmacokinetics. The 28 kDa conjugates cleared more rapidly from the blood and liver than the 60 and 121 kDa conjugates ($p < 0.05$). The 121 kDa conjugates showed relatively slow clearance as compared to those of 60 kDa, but the difference was not significant ($p > 0.05$) because of the low sensitivity of MRI. The 28 kDa conjugates showed rapid initial renal accumulation and clearance, while the conjugates with higher molecular weights exhibited low renal accumulation and slow clearance.

A relatively higher accumulation was observed in the tumor periphery than tumor interstitium for all conjugates, Fig. 5. No significant size effect on tumor accumulation was observed for the conjugates within the first 4 h post-injection, except the 28 kDa conjugates showed higher accumulation in tumor periphery within first 10 min post-injection ($p < 0.05$). However, higher tumor accumulation was observed for the conjugates with higher molecular weights at 24 and 48 h post-injection ($p < 0.05$). Tumor accumulation of the 28 kDa conjugates returned to the background level at 24 h post-injection.

Figure 6 shows the biodistribution of Gd(III) in the heart, liver, lung, kidneys, spleen, muscle and tumor in mice at 24 h for the 28 kDa conjugates and on day 7 for the conjugates of 60 and 121 kDa when the mice were sacrificed after the last MRI data acquisition. The conjugates with the same spacer showed size dependent accumulation in the organs and tissues except kidneys. At 24 h post-injection, the 28 kDa conjugates exhibited low accumulation in the liver, spleen, muscle and tumor as compared to the higher molecular weight conjugates at 7 days post-injection. PHPMA-GG-(Gd-DO3A) of 121 kDa had the highest accumulation in the heart, liver, lung, spleen, muscle and

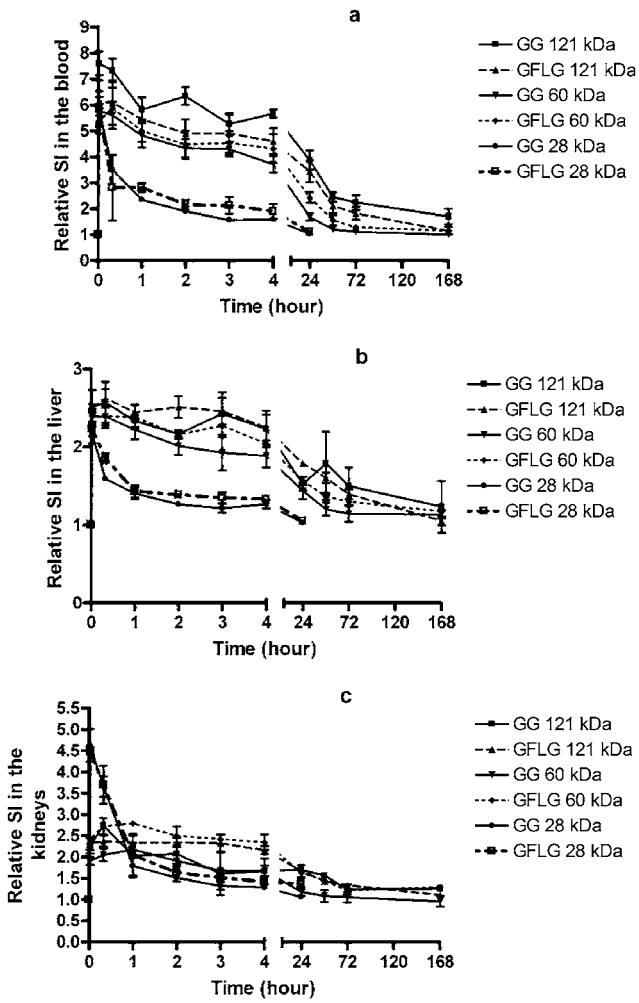

Fig. 4. Relative signal intensities in the blood (**a**), liver (**b**), and kidneys (**c**) at various time points after the injection of PHPMA-GG-(Gd-DO3A) and PHPMA-GFLG-(Gd-DO3A) conjugates.

tumor among all conjugates. PHPMA-GFLG-(Gd-DO3A) of 121 kDa showed significantly lower accumulation than PHPMA-GG-(Gd-DO3A) of 121 kDa in the liver, lung, spleen muscle and tumor ($p < 0.05$), possibly due to the presence of degradable spacer in PHPMA-GFLG-(Gd-DO3A). High uptake in spleen was observed for the high molecular weight conjugates possibly due to internalization of polymeric conjugates by macrophages. The conjugates of 60 and 121 kDa showed higher accumulation in tumor than in the heart, liver, kidney and muscle at 7 days postinjection.

DISCUSSION

The biodistribution, pharmacokinetics and tumor targeting efficiency of polymer drug conjugates are generally evaluated by conventional surgery based methods. A large number of experimental animals are sacrificed at a series of time points in order to obtain such pharmacokinetic and biodistribution data. We have shown in our previous publication and in this work that the real-time pharmacokinetics and biodistribution of the polymer conjugates labeled with stable Gd(III) chelates can be non-invasively and continuously visualized by the contrast enhanced MRI using a small number of experimental animals (12). Stable gadolinium(III) chelates have been used as contrast agents in magnetic resonance imaging to enhance the image contrast in tissues of interest (17,18). Contrast enhancement and MR signal intensity are non-linearly correlated to the concentration and relaxivities of the contrast agents (19). Therefore, there is a qualitative or semi-quantitative correlation that strong MR contrast signal intensity in the T_1-weighted MR images would represent high concentration of the contrast agents in the tissue. Although MR signal intensity is not linearly correlated to the concentration of the Gd(III) chelates in the conjugates, the conclusions drawn from the qualitative and semi-quantitative contrast enhanced MRI studies on the size effect of polymer conjugates are consistent to those reported using conventional methods (20,21).

In this study, the pharmacokinetics and biodistribution in major organs, tumor accumulation and excretion of the labeled PHPMA conjugates with narrow molecular weight distributions were visualized by contrast enhanced MRI with high spatial resolution. Dynamic contrast enhanced MRI showed the HPMA copolymer conjugates with lower molecular weights excreted more rapidly via renal filtration and had lower tumor targeting efficiency than the conjugates with higher molecular weights. Also the conjugates with higher molecular weights had longer blood circulation and higher tumor accumulation over time. Polymeric conjugates of 28 kDa had much lower tumor targeting efficiency than the 60 and 121 kDa conjugates. The size dependent tumor accumulation was also confirmed by the measurement of Gd in tumors at the end of the experiment. The observations from MRI studies were consistent with the results obtained from conventional methods, which further validates the feasibility of contrast enhanced MRI for non-invasive visualization of *in vivo* drug delivery of labeled polymer drug conjugates. However, the conventional pharmacokinetic study can only provides the average drug concentration in the target tissues. Dynamic contrast enhanced MRI provides continuous visualization of whole-body pharmacokinetics of the conjugates with high spatial resolution and the dynamic changes of heterogeneous accumulation in the tumor tissues.

The comparison of the data in this work to the previously published results (12) showed that HPMA copolymer conjugates with higher molecular weights had high tumor targeting efficiency than the poly(L-glutamic acid) with similar molecular weights or hydrodynamic volumes. For example, tumor accumulation of labeled poly(*L*-glutamic acid) with molecular weights of 50 and 87 kDa decreased from its peak accumulation at 24 h post-injection, while tumor accumulation of the PHPMA conjugates with medium and high molecular weights was much higher at the same time and remained at a high level for at least two more days. Biodegradability of poly(*L*-glutamic acid) may cause *in vivo* degradation of the conjugates and facilitate their clearance from the body, resulting in relatively low tumor accumulation. HPMA copolymer conjugates with high molecular weights were stable to *in vivo* degradation and had a longer blood circulation, resulting in relatively high and prolonged tumor accumulation.

HPMA copolymer conjugates with a degradable tetrapeptide, GlyPheLeuGly, were designed to study drug release from the conjugates. The tetrapeptide spacer would be degraded in the intracellular lysosomal compartments to release the contrast agent from the conjugates (22), possibly resulting in rapid excretion of the chelates and reduced MR signal intensity. However, no significant difference was observed by contrast enhanced MRI for the conjugates of different spacers in their blood pharmacokinetics, biodistribution and tumor targeting, possible due to the low sensitivity of MRI. The biodistribution study at the end of the MRI showed that the 121 kDa PHPMA conjugate with the degradable spacer had significantly lower Gd accumulation than that with the non-degradable spacer in the liver, lung, spleen and tumor ($p < 0.05$). This indicated that the degradable spacer is cleaved in the lysosomal compartments and the digestive organs to facilitate the release of the Gd chelate from the conjugates. No significant difference was observed for the conjugates with different spacers of lower molecular weights in the major organs or tissue except the liver, possibly due to the relative low tissue accumulation of the lower molecular weight conjugates.

Dynamic contrast enhanced MRI clearly revealed the size effect and structural properties (nondegradable polymers vs. biodegradable polymers) on pharmacokinetics, biodistribution and tumor targeting efficiency of polymer conjugates in an animal tumor model. However, the limitation of contrast enhanced MRI is its inherently low sensitivity and quantitative accuracy. Efforts are being made to develop reliable techniques for quantitative *in vivo* MR imaging, including T_1 mapping (23), which have a potential to accurately determine the concentration of MRI contrast agents *in vivo*. Nuclear imaging is highly sensitive for quantitative detection of labeled polymer conjugates, but limited by low spatial resolution and poor anatomic delineation. The combination of contrast enhanced MRI and nuclear imaging, e.g. SPECT, would provide a non-invasive method for non-invasive study of *in vivo* properties of polymer conjugates with high sensitivity and accuracy, and high spatial resolution. Dual imaging modalities with combination of MRI with SPECT or PET are now under development for both human and small animal imaging (24–26). Polymer conjugates can be readily labeled with both MRI contrast agent and gamma emitter for more accurate non-invasive *in vivo* studies with the dual imaging modalities.

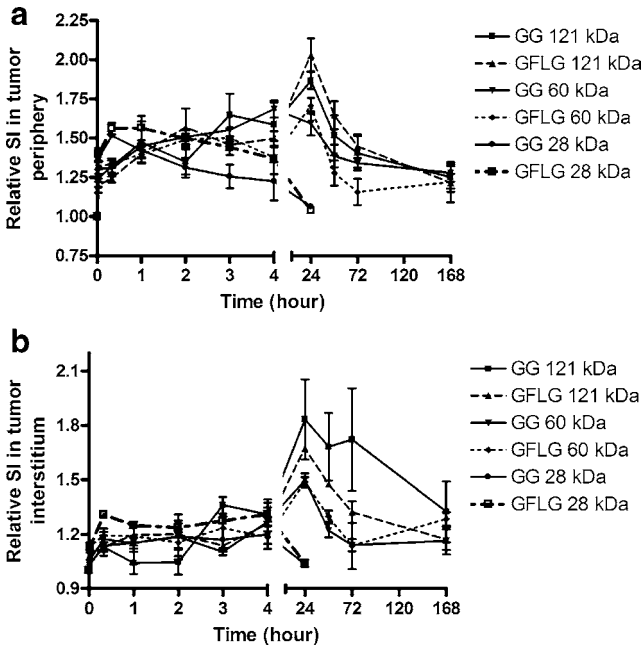

Fig. 5. Relative signal intensities in the tumor periphery (**a**) and tumor interstitium (**b**) at various time points after the injection of PHPMA-GG-(Gd-DO3A) and PHPMA-GFLG-(Gd-DO3A) conjugates.

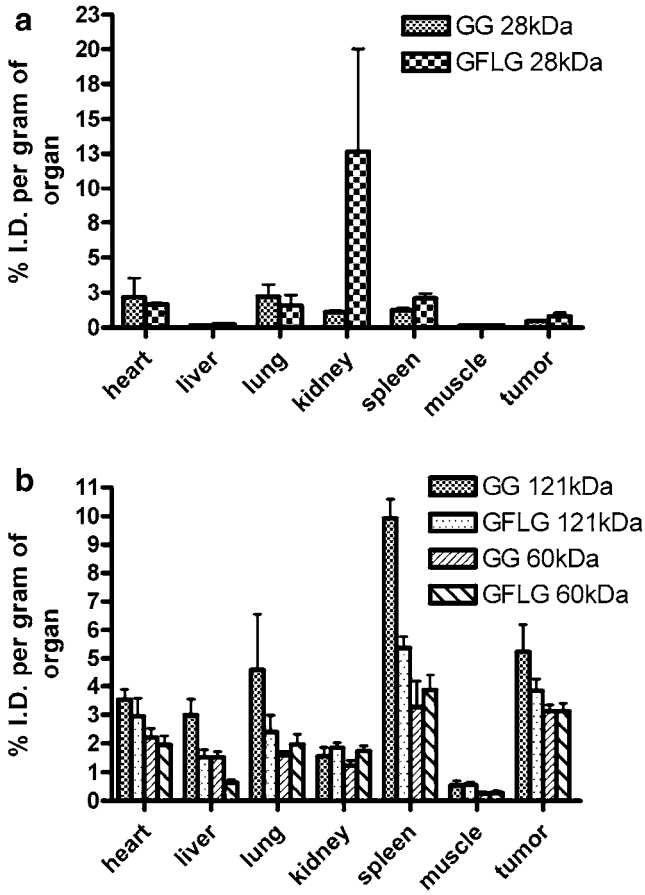

Fig. 6. Biodistribution of Gd(III) in mice at the end of the MRI studies, 24 h after intravenous injection of the conjugates of 28 kDa and 7 days for the conjugates of 60 and 121 kDa at a dose of 0.03 mmol-Gd/kg.

It has been reported that polymer anticancer drug conjugates with long blood circulation and slow excretion are more effective in anticancer therapy (27). Dynamic contrast enhanced MRI revealed that the polymer conjugates with higher molecular weights demonstrated more effective passive tumor targeting and prolonged tumor drug accumulation, moreover nondegradable biocompatible polymer conjugates were more efficient than the biodegradable polymer conjugates. These results would be valuable in the design and development of more efficient polymer anticancer conjugates for efficacious cancer treatment.

ACKNOWLEDGMENTS

This research was supported in part by NIH grant R01 CA097465. We thank Ms. Melody Johnson for the technical help in MRI data acquisition.

REFERENCES

1. J. Kopecek, P. Kopeckova, T. Minko, and Z.-R. Lu. HPMA copolymer-anticancer drug conjugates: design, activity, and mechanism of action. *Eur. J. Pharm. Biopharm.* **50**:61–81 (2000).
2. B. Rihova and K. Kubackova. Clinical implications of N-(2-hydroxypropyl)methacrylamide copolymers. *Curr. Pharm. Biotechnol.* **4**:311–322 (2003).
3. H. Maeda, L. W. Seymour, and Y. Miyamoto. Conjugates of anticancer agents and polymers: advantages of macromolecular therapeutics *in vivo*. *Bioconjug. Chem.* **3**:351–362 (1992).
4. R. Haag and F. Kratz. Polymer therapeutics: concepts and applications. *Angew. Chem. Int. Ed. Engl.* **45**:1198–1215 (2006).
5. Z.-R. Lu, J.-G. Shiah, P. Kopeckova, and J. Kopecek. Polymerizable Fab' antibody fragments targeted photodynamic cancer therapy in nude mice. *STP Pharm. Sci.* **13**:69–75 (2003).
6. M. V. Pimm, A. C. Perkins, J. Strohalm, K. Ulbrich, and R. Duncan. Gamma scintigraphy of the biodistribution of 123I-labelled N-(2-hydroxypropyl)methacrylamide copolymer-doxorubicin conjugates in mice with transplanted melanoma and mammary carcinoma. *J. Drug Target.* **3**:375–383 (1996).
7. P. J. Julyan, L. W. Seymour, D. R. Ferry, S. Daryani, C. M. Boivin, J. Doran, M. David, D. Anderson, C. Christodoulou, A. M. Young, S. Hesslewood, and D. J. Kerr. Preliminary clinical study of the distribution of HPMA copolymers bearing doxorubicin and galactosamine. *J. Control Release* **57**:281–290 (1999).
8. M. Kissel, P. Peschke, V. Subr, K. Ulbrich, J. Schuhmacher, J. Debus, and E. Friedrich. Synthetic macromolecular drug carriers: biodistribution of poly[(N-2-hydroxypropyl)methacrylamide] copolymers and their accumulation in solid rat tumors. *PDA J. Pharm. Sci. Technol.* **55**:191–201 (2001).
9. A. Mitra, A. Nan, H. Ghandehari, E. McNeill, J. Mulholland, and B. R. Line. Technetium-99m-Labeled N-(2-hydroxypropyl) methacrylamide copolymers: synthesis, characterization, and *in vivo* biodistribution. *Pharm. Res.* **21**:1153–1159 (2004).
10. M. V. Pimm, A. C. Perkins, J. Strohalm, K. Ulbrich, and R. Duncan. Gamma scintigraphy of a 123I-labelled N-(2-hydroxypropyl)methacrylamide copolymer-doxorubicin conjugate containing galactosamine following intravenous administration to nude mice bearing hepatic human colon carcinoma. *J. Drug Target.* **3**:385–390 (1996).
11. D. Wang, S. C. Miller, M. Sima, D. Parker, H. Buswell, K. C. Goodrich, P. Kopeckova, and J. Kopecek. The arthrotropism of macromolecules in adjuvant-induced arthritis rat model: a preliminary study. *Pharm. Res.* **21**:1741–1749 (2004).
12. F. Ye, T. Ke, E.-K. Jeong, X. Wang, Y. Sun, M. Johnson, and Z.-R. Lu. Noninvasive visualization of *in vivo* drug delivery of poly(L-glutamic acid) using contrast-enhanced MRI. *Mol. Pharmaceutics*. **3**:507–515 (2006).
13. K. Ulbrich, V. Subr, J. Strohalm, D. Plocova, M. Jelinkova, and B. Rihova. Polymeric drugs based on conjugates of synthetic and natural macromolecules. I. Synthesis and physico-chemical characterisation. *J. Control Release* **64**:63–79 (2000).
14. T. Ke, Y. Feng, J. Guo, D. L. Parker, and Z.-R. Lu. Biodegradable cystamine spacer facilitates the clearance of Gd(III) chelates in poly(glutamic acid) Gd-DOTA conjugates for contrast enhanced MR imaging. *Magn. Reson. Imaging*. **24**:931–940 (2006).
15. T. Kaneshiro, T. Ke, E. K. Jeong, D. L. Parker, and Z.-R. Lu. (Gd-DTPA)-(L-cystine bisalkylamide) copolymers as novel biodegradable macromolecular contrast agents for MR blood pool imaging. *Pharm. Res.* **23**:1285–1294 (2006).
16. Y. Feng, Y. Zong, T. Ke, and Z.-R. Lu. Pharmacokinetics and blood pool contrast enhancement of Gd-DTPA cystine copolymers and Gd-DTPA cystine diethyl ester copolymers. *Pharm. Res.* **23**:1736–1742 (2006).
17. P. Caravan, J. J. Ellison, T. J. McMurry, and R. B. Lauffer. Gadolinium(III) chelates as MRI contrast agents: structure, dynamics, and applications. *Chem. Rev.* **99**:2293–2352 (1999).
18. X. Wang, Y. Feng, T. Ke, M. Schabel, and Z.-R. Lu. Pharmacokinetics and tissue retention of (Gd-DTPA)-cystamine copolymers, a biodegradable macromolecular magnetic resonance imaging contrast agent. *Pharm. Res.* **22**:596–602 (2005).
19. P. L. Choyke, A. J. Dwyer, and M. V. Knopp. Functional tumor imaging with dynamic contrast-enhanced magnetic resonance imaging. *J. Magn. Reson. Imaging* **17**:509–520 (2003).
20. F. M. Veronese, O. Schiavon, G. Pasut, R. Mendichi, L. Andersson, A. Tsirk, J. Ford, G. Wu, S. Kneller, J. Davies, and R. Duncan. PEG-doxorubicin Conjugates: Influence of Polymer Structure on Drug Release, *in Vitro* Cytotoxicity, Biodistribution, and Antitumor Activity. *Bioconjug. Chem.* **16**:775–784 (2005).
21. L. W. Seymour, Y. Miyamoto, H. Maeda, M. Brereton, J. Strohalm, K. Ulbrich, and R. Duncan. Influence of molecular weight on passive tumour accumulation of a soluble macromolecular drug carrier. *Eur. J. Cancer* **31A**:766–770 (1995).
22. P. Rejmanova, J. Kopecek, R. Duncan, and J. B. Lloyd. Stability in rat plasma and serum of lysosomally degradable oligopeptide sequences in N-(2-hydroxypropyl) methacrylamide copolymers. *Biomaterials* **6**:45–48 (1985).
23. D. R. Messroghli, S. Plein, D. M. Higgins, K. Walters, T. R. Jones, J. P. Ridgway, and M. U. Sivananthan. Human myocardium: single-breath-hold MR T1 mapping with high spatial resolution-reproducibility study. *Radiology* **238**:1004–1012 (2006).
24. E. L. So. Integration of EEG, MRI, and SPECT in localizing the seizure focus for epilepsy surgery. *Epilepsia*. **41**(Suppl 3):S48–S54 (2000).
25. M. D. Seemann. Whole-body PET/MRI: the future in oncological imaging. *Technol. Cancer Res. Treat.* **4**:577–582 (2005).
26. S. W. Zielhuis, J. H. Seppenwoolde, V. A. Mateus, C. J. Bakker, G. C. Krijger, G. Storm, B. A. Zonnenberg, A. D. Schip, G. A. Koning, and J. F. Nijsen. Lanthanide-loaded liposomes for multimodality imaging and therapy. *Cancer Biother. Radiopharm.* **21**:520–527 (2006).
27. J. G. Shiah, M. Dvorak, P. Kopeckova, Y. Sun, C. M. Peterson, and J. Kopecek. Biodistribution and antitumour efficacy of long-circulating N-(2-hydroxypropyl)methacrylamide copolymer-doxorubicin conjugates in nude mice. *Eur. J. Cancer* **37**:131–139 (2001).